Electronic Supplementary Information for:

Porous Ni-Based Metal-Organic Frameworks Reduce the Oxygen Evolution Temperature of Lithium Perchlorate

Nicholas A. Tomalia,[a] *Yulia Rakova,*[a] *Ashley Tubman,*[a] *and Adam J. Matzger**[a,b]

[a]Department of Chemistry, University of Michigan, 930 North University Avenue, Ann Arbor, MI 48109, United States

[b]Macromolecular Science and Engineering Program, University of Michigan, Ann Arbor, MI 48109, United States

*To whom correspondence should be addressed. Email address: matzger@umich.edu

Table of Contents

S1. Characterization

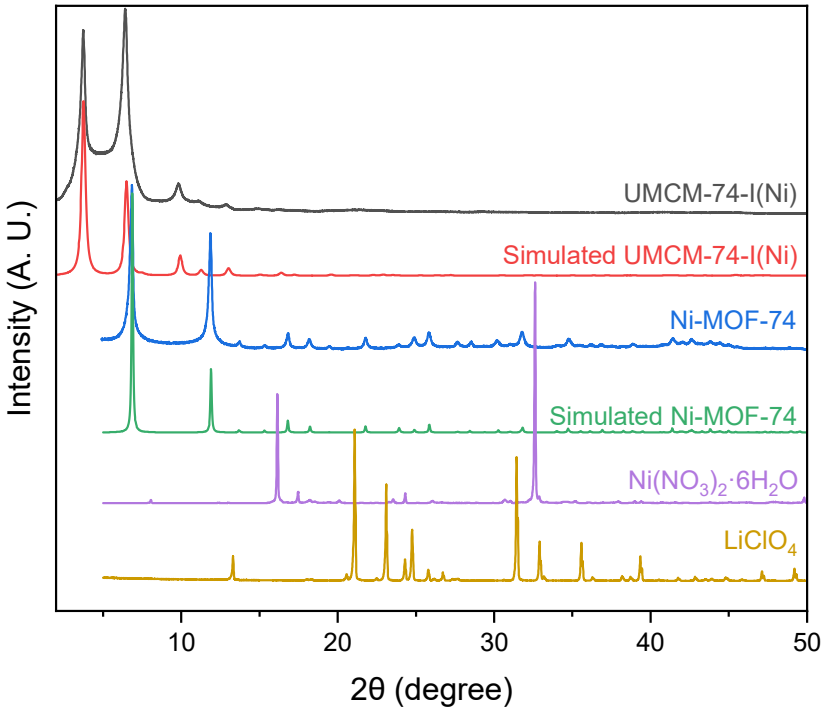

Figure S1. PXRD patterns of UMCM-74-I(Ni) (black), simulated UMCM-74-I(Ni)[1] (red), Ni-MOF-74 (blue), simulated Ni-MOF-74 (green; ref code: EWIZOC), $Ni(NO_3)_2 \cdot 6H_2O$ (purple), and $LiClO_4$ (gold).

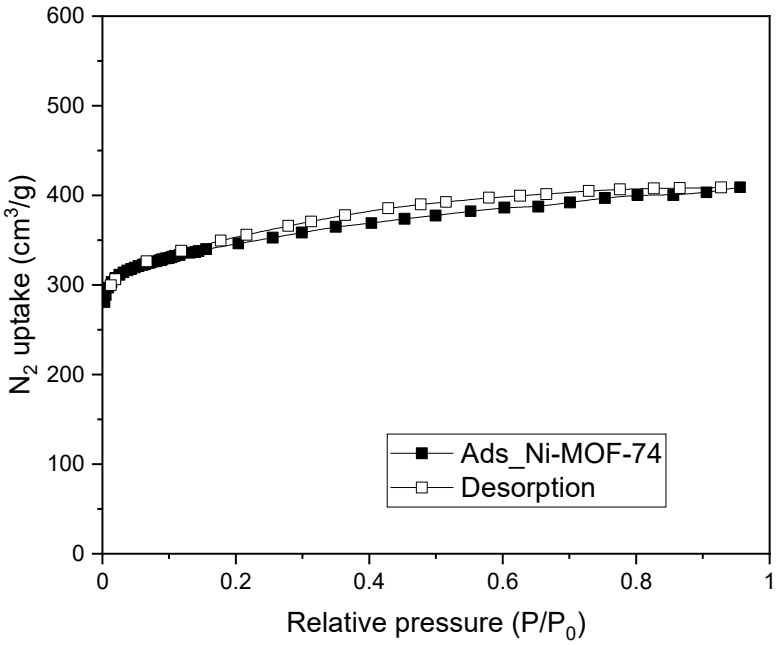

Figure S2. N_2 sorption isotherm for activated Ni-MOF-74, BET surface area = 1328 $m^2 g^{-1}$, pore volume = 0.57 $cm^3 g^{-1}$.

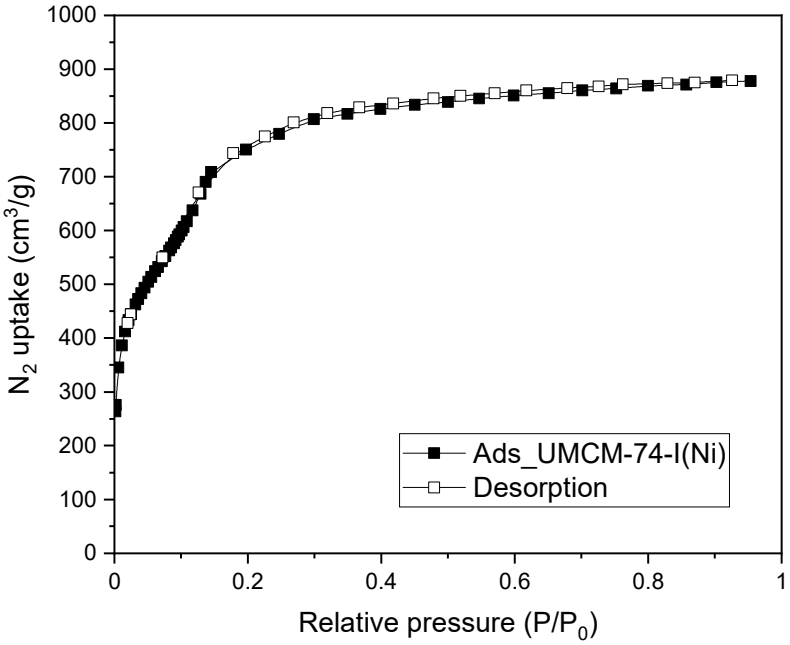

Figure S3. N_2 sorption isotherm for activated UMCM-74-I(Ni), BET surface area = 2479 m^2 g^{-1}, pore volume = 1.40 cm^3 g^{-1}.

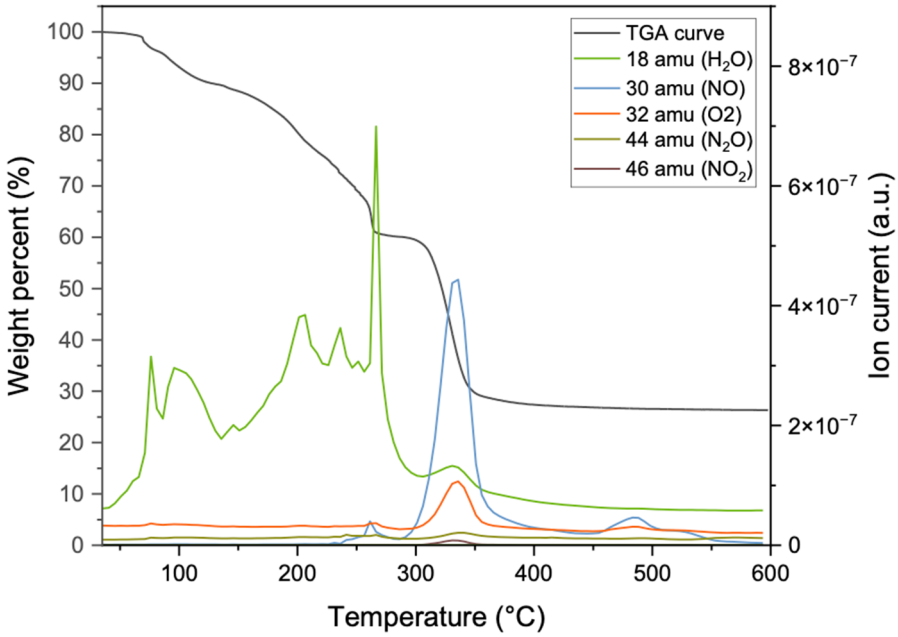

Figure S4. TGA-MS data collected for $Ni(NO_3)_2 \cdot 6H_2O$ showing the weight loss associated with dehydration and subsequent decomposition (black) and the monitored *m/z* for H_2O (green), NO (blue), O_2 (orange), N_2O (olive green), and NO_2 (brown).

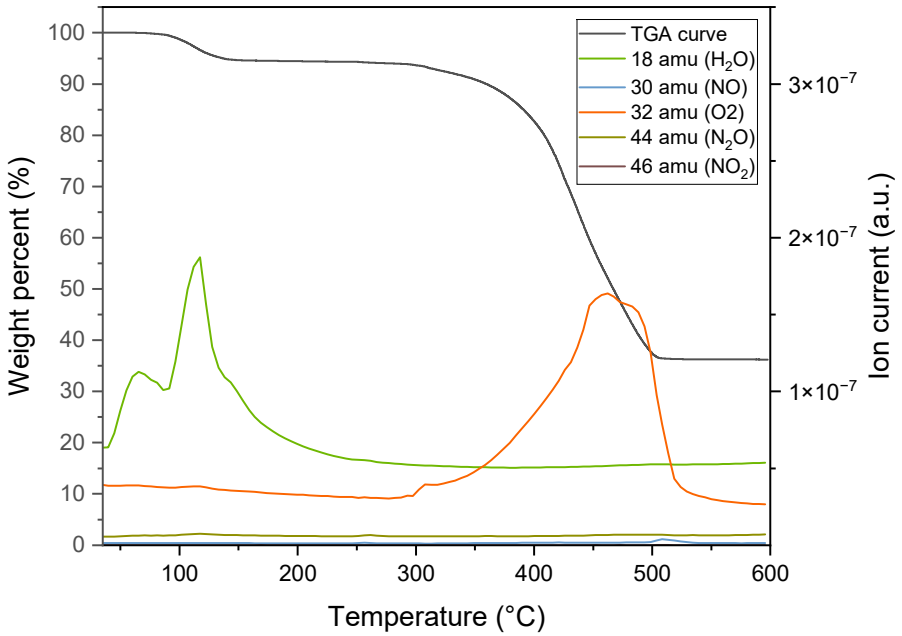

Figure S5. TGA-MS data collected for $LiClO_4/Ni(NO_3)_2{\cdot}6H_2O$ mixture with 0.42 wt% Ni content showing the weight loss associated with dehydration and subsequent decomposition (black) and the monitored *m/z* for H_2O (green), NO (blue), O_2 (orange), N_2O (olive green), and NO_2 (brown). During decomposition 0.3 mol% H_2O, 0.7 mol% NO, 0.4 mol% N_2O, and 98.6 mol% O_2 is detected by MS.

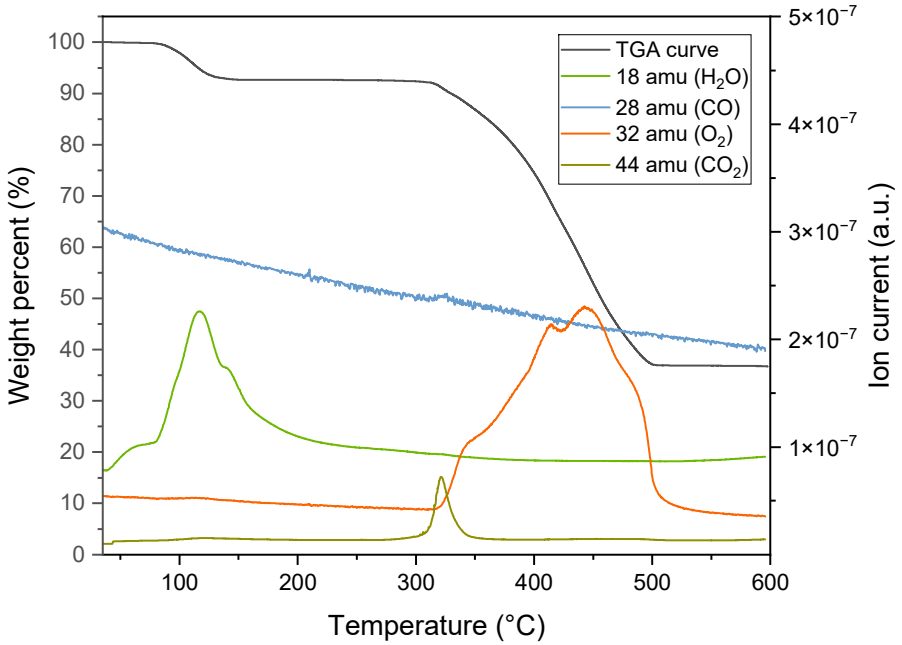

Figure S6. TGA-MS data collected for $LiClO_4$/Ni-MOF-74 mixture with 0.42 wt% Ni content showing the weight loss associated with dehydration and subsequent decomposition (black) and the monitored *m/z* for H_2O (green), CO (blue), O_2 (orange), and CO_2 (olive green). During decomposition 0.2 mol% CO, 2.5 mol% CO_2, and 97.3 mol% O_2 is detected by MS.

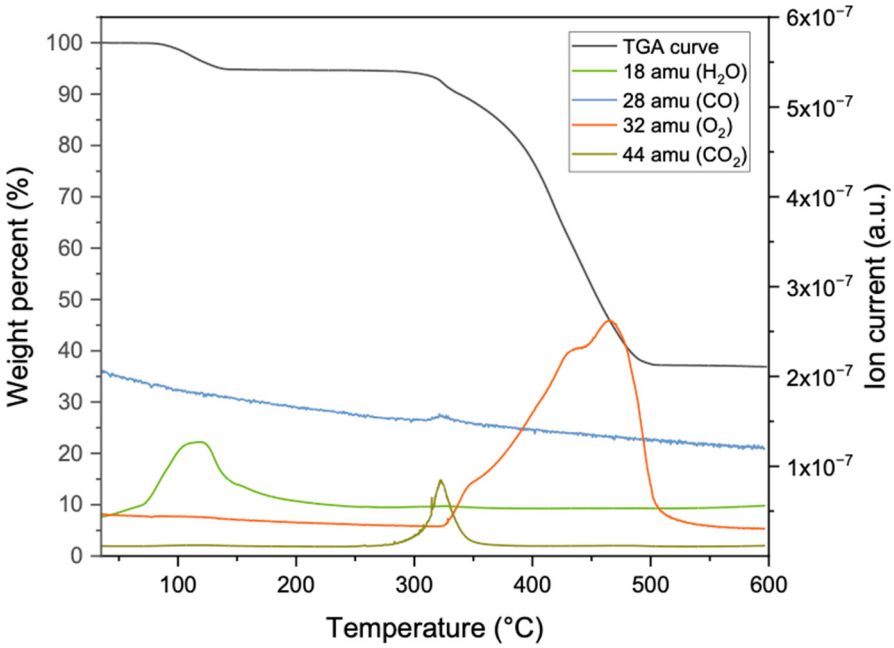

Figure S7. TGA-MS data collected for $LiClO_4$/UMCM-74-I(Ni) mixture with 0.42 wt% Ni content showing the weight loss associated with dehydration and subsequent decomposition (black) and the monitored *m/z* for H_2O (green), CO (blue), O_2 (orange), and CO_2 (olive green). During decomposition 0.4 mol% CO, 4.4 mol% CO_2, and 95.2 mol% O_2 is detected by MS.

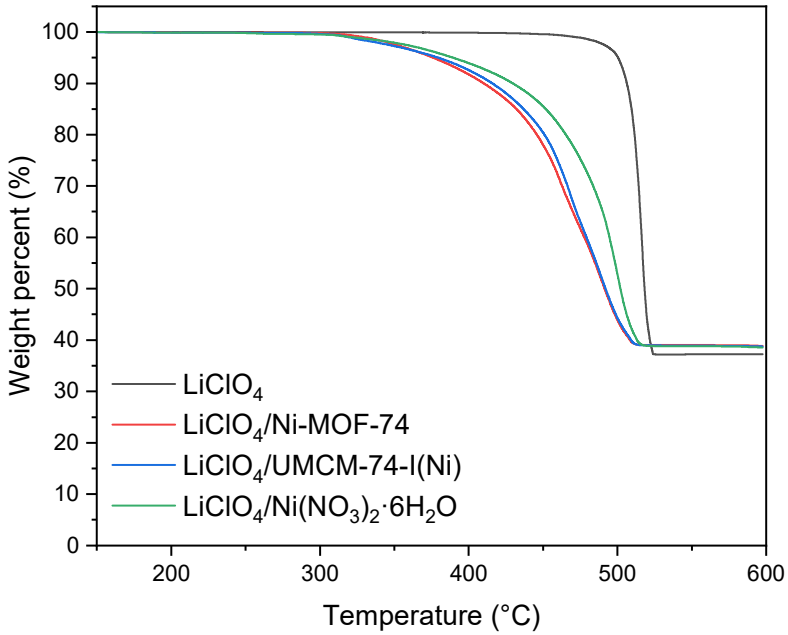

Figure S8. TGA thermograms (10 °C/min) showing the decomposition of pure $LiClO_4$ (black) and $LiClO_4$/Ni-MOF-74 (red), $LiClO_4$/UMCM-74-I(Ni) (blue), and $LiClO_4/Ni(NO_3)_2{\cdot}6H_2O$ (green) mixtures containing 0.21 wt% Ni loading after dehydration.

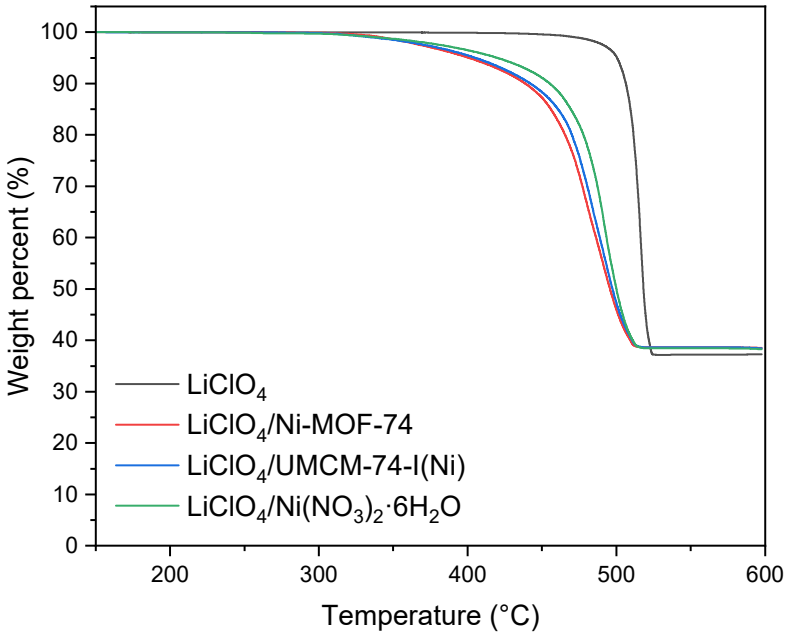

Figure S9. TGA thermograms (10 °C/min) showing the decomposition of pure $LiClO_4$ (black) and $LiClO_4$/Ni-MOF-74 (red), $LiClO_4$/UMCM-74-I(Ni) (blue), and $LiClO_4/Ni(NO_3)_2{\cdot}6H_2O$ (green) mixtures containing 0.10 wt% Ni loading after dehydration.

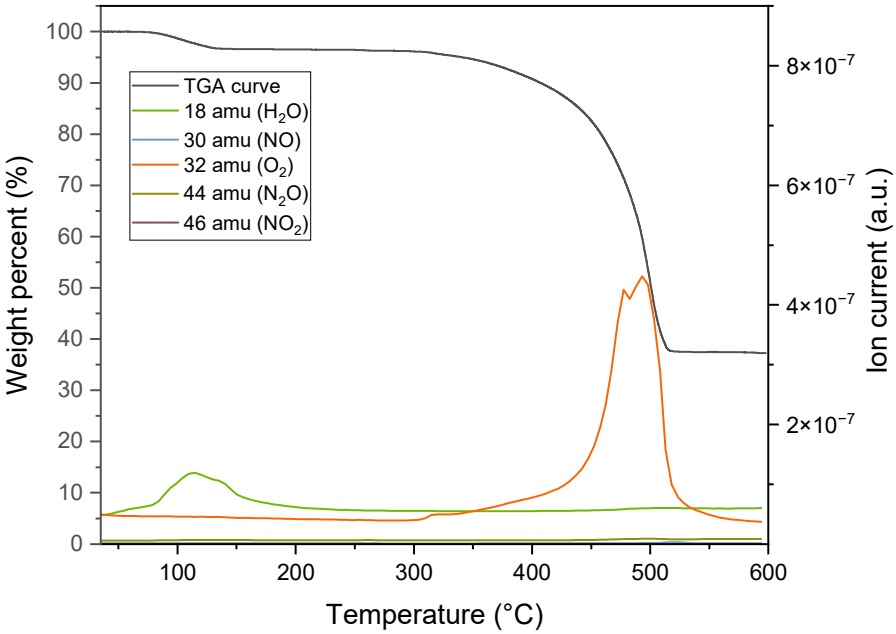

Figure S10. TGA-MS data collected for $LiClO_4/Ni(NO_3)_2{\cdot}6H_2O$ mixture with 0.21 wt% Ni content showing the weight loss associated with dehydration and subsequent decomposition (black) and the monitored *m/z* for H_2O (green), NO (blue), O_2 (orange), N_2O (olive green), and NO_2 (brown). During decomposition 0.2 mol% H_2O, 0.4 mol% NO, 0.2 mol% N_2O, and 99.2 mol% O_2 is detected by MS.

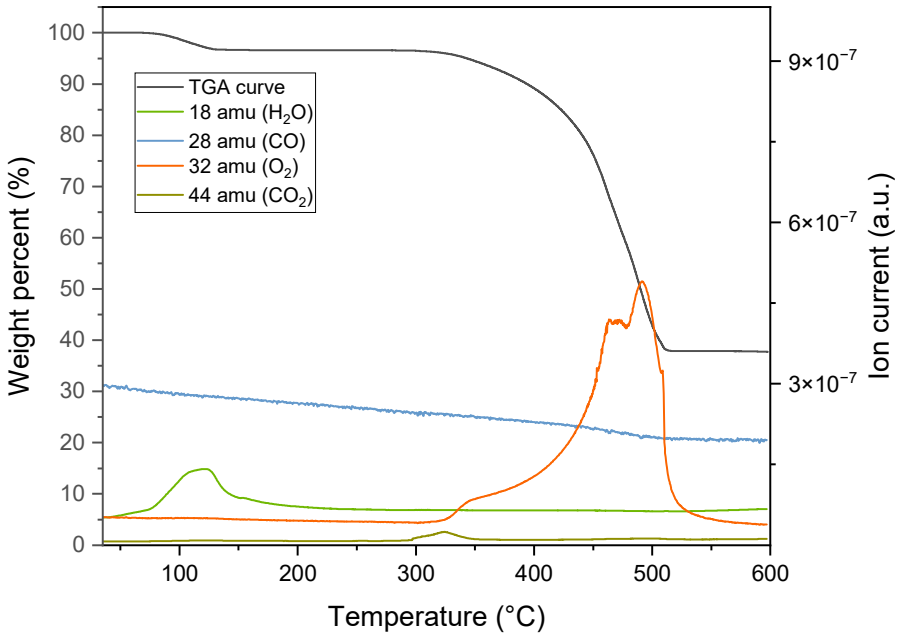

Figure S11. TGA-MS data collected for $LiClO_4$/Ni-MOF-74 mixture with 0.21 wt% Ni content showing the weight loss associated with dehydration and subsequent decomposition (black) and the monitored *m/z* for H_2O (green), CO (blue), O_2 (orange), and CO_2 (olive green). During decomposition 0.1 mol% CO, 1.3 mol% CO_2, and 98.6 mol% O_2 is detected by MS.

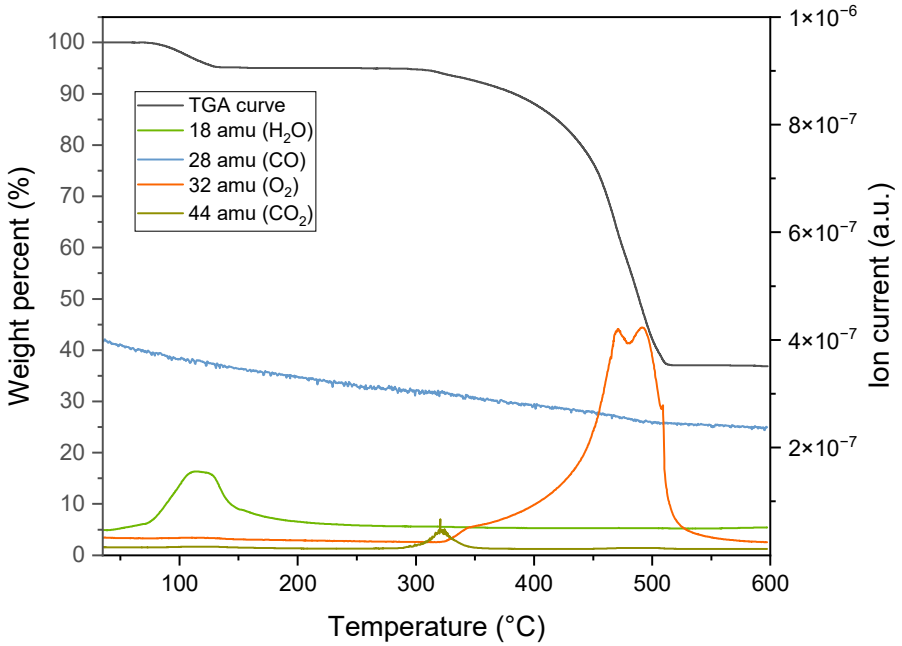

Figure S12. TGA-MS data collected for $LiClO_4$/UMCM-74-I(Ni) mixture with 0.21 wt% Ni content showing the weight loss associated with dehydration and subsequent decomposition (black) and the monitored *m/z* for H_2O (green), CO (blue), O_2 (orange), and CO_2 (olive green). During decomposition 0.2 mol% CO, 2.1 mol% CO_2, and 97.7 mol% O_2 is detected by MS.

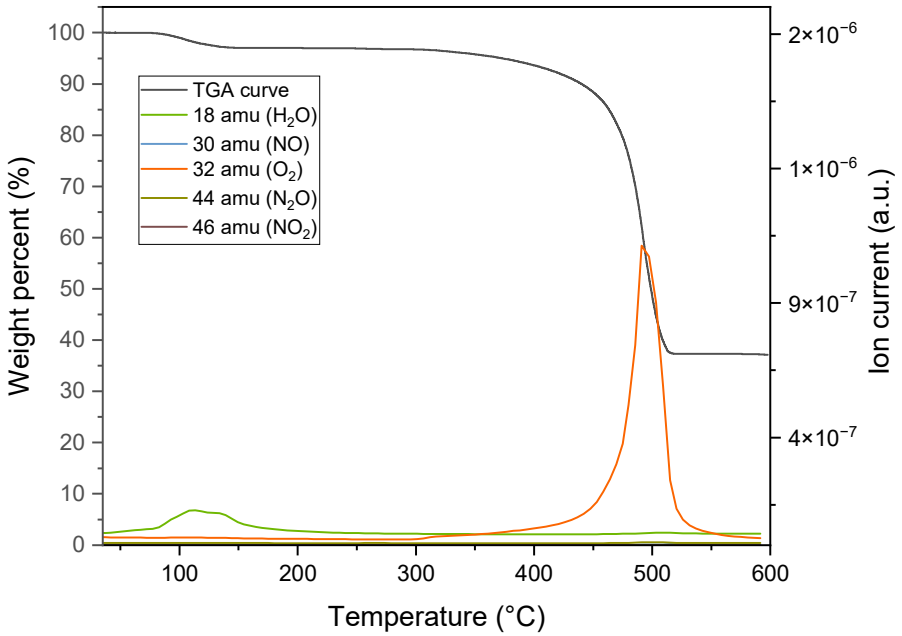

Figure S13. TGA-MS data collected for $LiClO_4/Ni(NO_3)_2{\cdot}6H_2O$ mixture with 0.10 wt% Ni content showing the weight loss associated with dehydration and subsequent decomposition (black) and the monitored *m/z* for H_2O (green), NO (blue), O_2 (orange), N_2O (olive green), and NO_2 (brown). During decomposition 0.1 mol% H_2O, 0.1 mol% NO, 0.1 mol% N_2O, and 99.7 mol% O_2 is detected by MS.

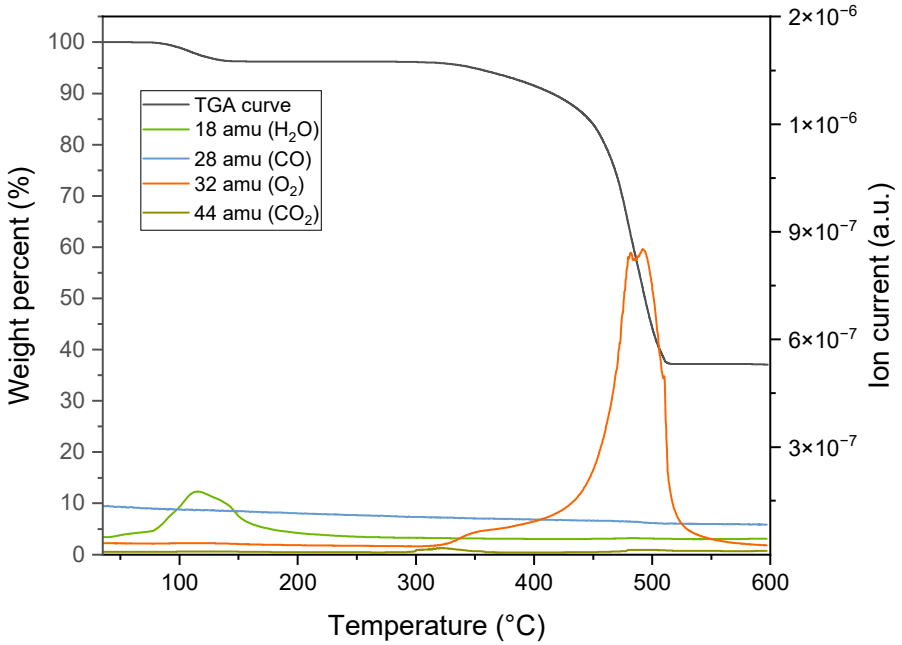

Figure S14. TGA-MS data collected for $LiClO_4$/Ni-MOF-74 mixture with 0.10 wt% Ni content showing the weight loss associated with dehydration and subsequent decomposition (black) and the monitored *m/z* for H_2O (green), CO (blue), O_2 (orange), and CO_2 (olive green). During decomposition 0.05 mol% CO, 0.64 mol% CO_2, and 99.31 mol% O_2 is detected by MS.

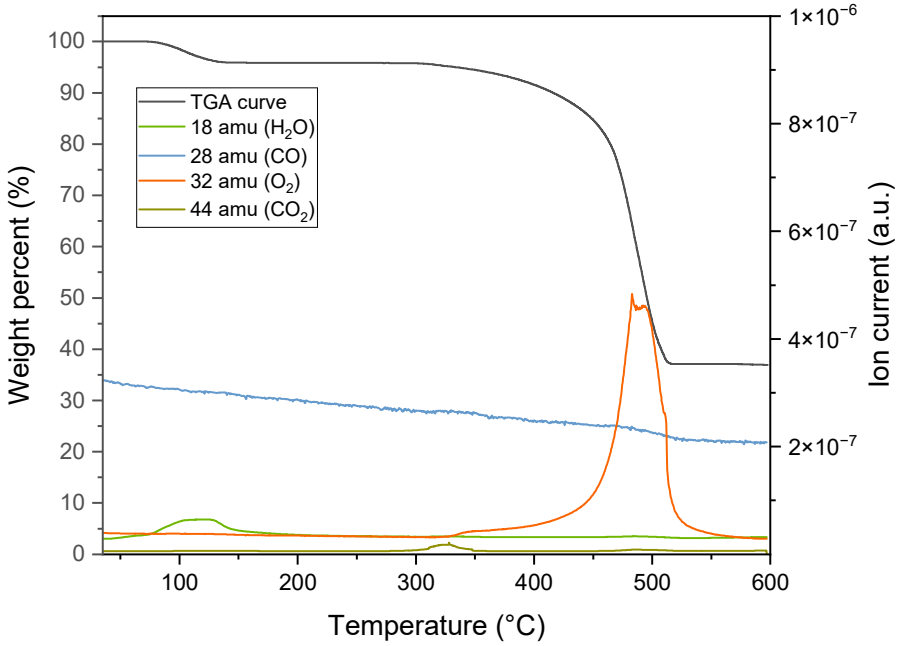

Figure S15. TGA-MS data collected for $LiClO_4$/UMCM-74-I(Ni) mixture with 0.10 wt% Ni content showing the weight loss associated with dehydration and subsequent decomposition (black) and the monitored *m/z* for H_2O (green), CO (blue), O_2 (orange), and CO_2 (olive green). During decomposition 0.10 mol% CO, 1.1 mol% CO_2, and 98.8 mol% O_2 is detected by MS.

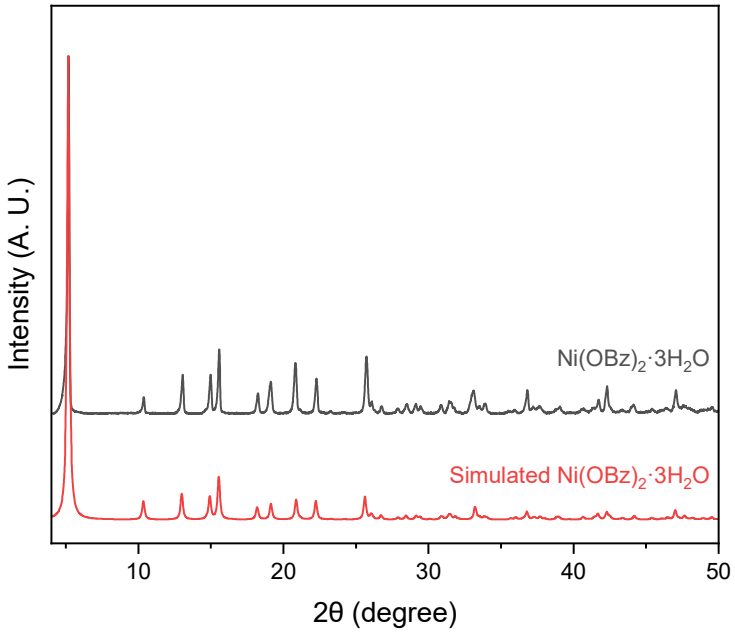

Figure S16. PXRD patterns of $Ni(OBz)_2{\cdot}3H_2O$ (black) and simulated $Ni(OBz)_2{\cdot}3H_2O$ (red; ref code: EJEDAA).

S2. Bimetallic catalyst study

To assess potential bimetallic catalytic synergy for $LiClO_4$ decomposition, $LiClO_4$ samples containing ~2 wt% catalyst mixtures (relative to composite) were prepared using equimolar combinations of $Ni(NO_3)_2{\cdot}6H_2O$ and 14 different metal salts (Table S1). $LiClO_4$ and the corresponding metal salts were dissolved in 1 mL of DI H_2O in 4 mL glass vials, vortex mixed, and dried at 90 °C overnight to yield physical mixtures. The thermal decomposition of each $LiClO_4$/bimetallic catalyst mixture was evaluated by TGA and compared to a control sample containing 2 wt% $Ni(NO_3)_2{\cdot}6H_2O$. Among the $Ni(NO_3)_2{\cdot}6H_2O$/metal salt combinations examined, only the $Sm(NO_3)_3{\cdot}6H_2O$/$Ni(NO_3)_2{\cdot}6H_2O$ exhibited a modest decrease in decomposition onset, midpoint, and completion temperatures relative to the $Ni(NO_3)_2{\cdot}6H_2O$ control (vide infra), although these values remained higher than those observed for $LiClO_4$/MOF compositions at the same Ni loading (0.42 wt%) as the $Ni(NO_3)_2{\cdot}6H_2O$ control sample (Figure S16). While this result suggests a minor bimetallic synergistic effect relative to the $Ni(NO_3)_2{\cdot}6H_2O$ control, the improvement was insufficient to justify incorporation of a second catalyst into the Ni-based MOFs, and the Sm-containing bimetallic catalyst mixture remained less effective than the porous Ni-based MOFs alone.

	T_d onset (°C)	T_d midpoint (°C)	T_d completion (°C)
$Ni(NO_3)_2 \cdot 6H_2O$ (control)	372	461	509
$Sm(NO_3)_3 \cdot 6H_2O$ / $Ni(NO_3)_2 \cdot 6H_2O$	358	456	501
$Co(NO_3)_2 \cdot 6H_2O$ / Ni(NO3)2 6H20	381	462	507
$Al(NO_3)_2 \cdot 9H_2O$ / $Ni(NO_3)_2 \cdot 6H_2O$	380	479	515
$Ce(NO_3)_2 \cdot 6H_2O$ / $Ni(NO_3)_2 \cdot 6H_2O$	390	470	512
LiCl / $Ni(NO_3)_2 \cdot 6H_2O$	397	471	516
$SnCl_2$ / $Ni(NO_3)_2 \cdot 6H_2O$	410	472	516
$Cu(NO_3)_2 \cdot 2.5H_2O$ / Ni(NO3)2 6H20	446	483	514
$Mn(NO_3)_2 \cdot 4H_2O$ / Ni(NO3)2 6H20	452	485	512
$Mg(NO_3)_2 \cdot 6H_2O$ / Ni(NO3)2 6H20	455	491	518
$TiOSO_4 \cdot xH_2O$ / $Ni(NO_3)_2 \cdot 6H_2O$	466	488	518
$Zn(NO_3)_2 \cdot 6H_2O$ / $Ni(NO_3)_2 \cdot 6H_2O$	469	492	517
$Sr(NO_3)_2$ / $Ni(NO_3)_2 \cdot 6H_2O$	470	487	521
$Fe(NO_3)_2 \cdot 9H_2O$ / Ni(NO3)2 6H20	476	492	519
$(NH_4)_6Mo_7O_{24} \cdot 9H_2O$ / $Ni(NO_3)_2 \cdot 6H_2O$	499	511	526

Table S1. Thermal decomposition (T_d) onset, midpoint, and completion temperatures measured by TGA at 10 °C/min for samples of $LiClO_4$ containing ~2 wt% catalyst mixtures comprising equimolar ratios of $Ni(NO_3)_2 \cdot 6H_2O$ and 14 different metal salts.

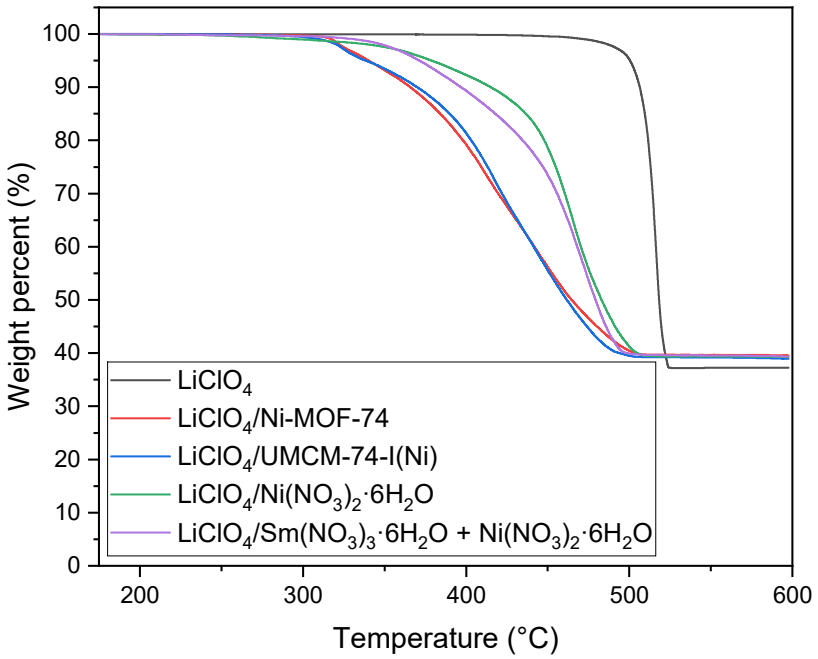

Figure S17. TGA thermograms (°C/min) showing decomposition of pure $LiClO_4$ (black) and $LiClO_4$ mixtures with Ni-MOF-74 (red), UMCM-74-I(Ni) (blue), and $Ni(NO_3)_2{\cdot}6H_2O$ (green) at 0.42 wt% Ni loading, along with $LiClO_4$ containing a ~2 wt% equimolar $Sm(NO_3)_3{\cdot}6H_2O/Ni(NO_3)_2{\cdot}6H_2O$ bimetallic catalyst (post-dehydration).

S3. References

(1) Tomalia, N. A.; Rakova, Y.; Tubman, A. N.; Matzger, A. J. Tunable On-Demand Explosives Derived from Isoreticular Metal–Organic Framework Nanocomposites. *Chem. Mater.* **2026**, *38* (4), 2055–2062. https://doi.org/10.1021/acs.chemmater.5c03363.